Endogenous CO_2 ice mixture on the surface of Europa and no detection of plume activity

G. L. Villanueva[1,*], H. B. Hammel[2], S. N. Milam[1], S. Faggi[1,3], V. Kofman[1,3], L. Roth[4], K. P. Hand[5], L. Paganini[6], J. Stansberry[7], J. Spencer[8], S. Protopapa[8], G. Strazzulla[9], G. Cruz-Mermy[10], C. R. Glein[11], R. Cartwright[12], G. Liuzzi[13]

[1] NASA Goddard Space Flight Center, Greenbelt MD 20771, USA

* Corresponding author: geronimo.villanueva@nasa.gov

[2] Association of Universities for Research in Astronomy, Washington DC 20004, USA

[3] American University, Washington, DC 20016, USA

[4] Royal Institute of Technology, Stockholm 104 50, Sweden

[5] Jet Propulsion Laboratory, Pasadena CA 91109, USA

[6] NASA Headquarters, Washington DC 20546, USA

[7] Space Telescope Science Institute, Baltimore MD 21218, USA

[8] Southwest Research Institute, Boulder CO 80302, USA

[9] Osservatorio Astrofisico di Catania, Istituto Nazionale di Astrofisica, 95123 Catania, Italy

[10] Universite Paris-Sarclay, 91190 Gif-sur-Yvette, France

[11] Southwest Research Institute, San Antonio TX 78238, USA

[12] Carl Sagan Center for Research, Search for Extraterrestrial Intelligence Institute, Mountain View CA 94043, USA

[13] Università degli Studi della Basilicata, 85100 Potenza, Italy

Published in Science on September 21st 2023

https://www.science.org/journal/science

Jupiter's moon Europa has a sub-surface ocean beneath an icy crust. Conditions within the ocean are unknown, and it is unclear whether it is connected to the surface. We observed Europa with the James Webb Space Telescope (JWST) to search for active release of material by probing its surface and atmosphere. A search for plumes yielded no detection of water, carbon monoxide, methanol, ethane, nor methane fluorescence emissions. Four spectral features of CO_2 ice were detected; their spectral shapes and distribution across Europa's surface indicate the CO_2 is mixed with other compounds and concentrated in Tara Regio. The $^{13}CO_2$ absorption is consistent with an isotopic ratio of $^{12}C/^{13}C = 83 \pm 19$. We interpret these observations as indicating that carbon is sourced from within Europa.

Jupiter's moon Europa is thought to host a subsurface ocean beneath a surface icy crust, which has a thickness estimated to be between 23 and 47 km (*1*). Spacecraft measurements have shown Europa has an induced magnetic field, which has been interpreted as due to a deep salty ocean (*2*, *3*). Smaller liquid water bodies might also be present within the ice shell (*4*). Europa's surface is one of the youngest in the Solar System, with the near absence of impact craters indicating an age in the range of 40 to 90 million years old (*5*). The extensive resurfacing is probably due to tidal heating sustained by orbital resonance, which could power cryovolcanism (*6*) where water and volatiles are erupted through the ice crust at freezing temperatures, and the upwelling of material forming ice domes (*7*). These processes would provide pathways for subsurface materials to reach the surface, where they could be observed.

Surface materials could be either endogenous (from within Europa) or exogenous (delivered by impacts or from Jupiter's magnetosphere); distinguishing between these possibilities is required to infer properties of the subsurface ocean (*8*). Europa's surface composition is dominated by water ice (*9*), with a complex mixture of other compounds, including salts (e.g., NaCl, hydrated sulfates) (*10*, *11*), and carbon- and sulfur-bearing molecular species (*12–14*). The diversity of observed species leads to uncertainty about the endogenous or exogenous nature of material on Europa's surface.

Searches for plume activity

A possible indication of endogenic material on Europa would be plumes, ejections of large amounts of material through cracks in the ice opened by the strong tidal forces. Evidence for plumes has been reported using ultraviolet observations of auroral emission lines of hydrogen and oxygen in the southern hemisphere, which were interpreted as due to localized plumes containing up to 1×10^{32} molecules of H_2O (*15*). This plume activity has not been confirmed by subsequent observations despite several attempts. Magnetic field and plasma wave observations from a close spacecraft flyby of Europa were interpreted as due to a plume (*16*). Transit observations of the Europa limb have been also interpreted as localized excess emission (*17*), or alternatively as statistical noise, not plume activity (*18*). Another study identified one tentative detection (at the 3-sigma level) of water vapor plume activity, within an otherwise quiescent period (*19*).

To search for active sources on Europa, we probed its atmosphere and surface using JWST (*20*), performing imaging with NIRCam (Near Infrared Camera) and spectroscopy in the 2.4–5.2 μm spectral range (Fig. 1) with NIRSpec (Near Infrared Spectrograph) at a resolving power of ~2700. The observations took place on 2022 November 23 and sample Europa's leading hemisphere (*21*). Searching for plume activity was done by probing the narrow molecular infrared features fluorescing in sunlight. We targeted the strong fundamentals bands of H_2O at 2.7 µm; CH_4, C_2H_6 and CH_3OH in the C-H stretch region (near 3.3 µm); and CO at 4.7 µm. We extracted an integrated spectrum across a 1.3″ diameter region centered on Europa (500 km beyond its radius), sampling the extended region beyond the 1″ moon's diameter. We then removed solar and ice absorption features and compared the resulting residual spectra (Fig. S1) to line-by-line fluorescence models by performing retrievals (*21*). We assumed an excitation rotational temperature of 25 K in the models, similar to the value measured in the plume of Enceladus (*22*). None of the targeted molecules were detected in the Europa spectrum, and the resulting 3σ upper limits, in units of 10^{30} molecules, are <35 for H_2O, <18 for CH_4, <18 for C_2H_6, <93 for CH_3OH, and <14 for CO. Assuming an outgassing velocity of 583 m s^{-1} (*19*) and isotropic outflow, the upper-limit of water (<35×10^{30} H_2O molecules) corresponds to a water vapor plume activity lower than 1×10^{28} molecule s^{-1} (<300 kg s^{-1}). This upper-limit for water is a factor of two times lower than the previous tentative detection in the leading hemisphere [$(70\pm22)\times10^{30}$ H_2O molecules (*19*)]; a factor of four times lower than inferred from auroral ultraviolet emission lines on the anti-Jovian hemisphere [$(130\pm30)\times10^{30}$ H_2O molecules (*15*)]; and five times lower than the median value [180×10^{30} H_2O molecules] reported for plumes at the trailing hemisphere (*17*). The JWST observations of the leading hemisphere set a limit on sustained water plume activity on Europa; if any plume activity exists on Europa today, it must be localized and weak (*16*), infrequent and not active during our observations, or devoid of the volatile gases that we searched for.

CO_2 detection and isotope ratio

An alternative way to probe for endogenic sources on Europa is to search for recently deposited material on its surface. The NIRCam images (Fig. 2A), obtained by combining the observations with filters F140M [1.331 to 1.479 μm] and F212N [2.109 to 2.134 μm], show enhanced brightness in Tara Regio (10°S, 75°W), an area of chaos terrain; and on the anti-Jovian side of Europa (180°W). The chaos terrain is an area of irregular groups of large blocks, which are thought to be related to an active geological process. Using the contemporaneously collected NIRSpec spectra of the leading hemisphere, we searched for evidence of CO, CH_4 or CH_3OH ices, but did not detect them. It has been suggested that CO_2 ice on Europa is concentrated on the anti-Jovian and trailing sides of its surface (*12*), however the absorption bands were only marginally resolved in earlier data (*23*). Many non-water ice bands have previously been mapped at hemisphere scales, including H_2O_2 at 3.5 μm (*24*), CO_2 at 4.3 μm (*12*) and SO_2 at 4.0 μm (*12*, *25*). If CO_2 is associated with endogenic landforms, then it would provide information on Europa's interior, such as the carbon content of the ocean. Theoretical models have predicted that the ocean contains dissolved CO_2 and other carbonate species (*26*), yet observations in the near infrared (1–2.5 μm) did not detect CO_2 (*27*) on Europa, so its presence and distribution remain unclear.

In the JWST data, we detect multiple features due to CO_2 ice on Europa: a narrow absorption band at 2.7 μm (Fig. 1B), a double-peaked absorption band at 4.25 and 4.27 μm (Fig. 1C), and an absorption due to the isotopologue $^{13}CO_2$ at 4.38 μm (Fig. S2C). $^{13}CO_2$ has previously been observed on two of Saturn's moons, Phoebe and Iapetus (*28*), but not on Europa. From the ratio of the $^{12}CO_2$ and $^{13}CO_2$ features, we estimate the carbon isotopic ratio $^{12}C/^{13}C = 83 \pm 19$ (1σ)

(*21*). This value is consistent with the Earth inorganic standard (Vienna Peedee Belemnite [VPDB]) which has $^{12}C/^{13}C = 89$ (*29*). It is also consistent with measured values for Iapetus $^{12}C/^{13}C = 83 \pm 8$ (*28*) and with the range of $^{12}C/^{13}C$ ratios, between 83 and 85, measured from carbonate minerals in Ivuna-type carbonaceous chondrite meteorites and samples of the asteroid Ryugu (*30*). These values could reflect primordial (present in the protosolar nebular) CO_2 which could have been incorporated into Europa, if it assembled from materials that formed at temperatures below ~80 K (*31*). Alternatively, the carbon in Europa's CO_2 could have been inherited from accreted primitive organic matter in the Solar System, which has $^{12}C/^{13}C = 90 \pm 1$ (*32*). The ratio of ^{13}C to ^{12}C is used as a biosignature on Earth (*33*), where localized carbon sources and reservoirs can have higher $^{12}C/^{13}C$ ratios (up to 104) due to biogenic processes (*29*). For C isotopes to serve as a biosignature on Europa, the isotopic fractionation between reduced carbon and CO_2 would need to be determined (*34*), which we cannot measure using these data and therefore we cannot distinguish between abiotic or biogenic sources.

Nature and distribution of the CO_2 ice

The observed 4.25 μm absorption band due to $^{12}CO_2$ has a double-peaked structure, which differs from the single-peaked crystalline CO_2 ice (see Fig. 1C). The synthetic spectrum of crystalline CO_2 ice in Fig. 1C was computed with the surface model of the Planetary Spectrum Generator (PSG) (*21*, *35*). The best match we found to this doubly peaked shape (Fig. 1C) was to a laboratory spectrum of a mixture of CO_2, H_2O, and CH_3OH in the ratio 1:0.8:0.9 respectively, measured at a temperature of 114 K (*36*). The temperature of this laboratory spectrum is within the range previously measured for different hemispheres of Europa (90 to 130 K) (*37*). This could indicate that CO_2 is stored in a water and organic-rich matrix on Europa, yet we did not detect any bands in our spectra due to CH_3OH ice or other organic molecules. We regard methanol as a proxy for the effect of any organics on the band position of CO_2, and several other effects could also produce shifts in the CO_2 fundamental band (*21*, *38*). A blue-shifted CO_2 peak has previously been observed on Ganymede and Callisto (*39*, *40*), but did not show the same double peak signature as we observe on Europa, perhaps due to differing spectral resolutions. The closest match to the CO_2 band detected on Callisto and Ganymede was a laboratory spectrum of carbonic acid (H_2CO_3), synthesized in a CO_2:H_2O ice mixture (in the ratio 5:1), then exposed to ionizing radiation in the form of 5 keV electrons (*41*). Similar laboratory irradiation experiments have been reported for Europa-like conditions (*42*). Fig. 1C shows a synthetic spectrum based on the carbonic acid experiment (*41*), which reproduces the width and location of the band, but not its double peak. To further test a possible matrix for the observed CO_2, we measured spectra of oceanic salt evaporite with a thin CO_2 ice film deposited onto the salts at different temperatures while being irradiated (*21*). In the experiments, the feature at 4.25 μm appeared after irradiation of the salts, while the feature at 4.27 μm was present in freshly deposited CO_2. We therefore interpret the 4.25 μm band as likely indicating CO_2 either adsorbed onto salts or captured within them.

We searched for heterogeneities in the CO_2 ice abundance and its structure, by mapping the strengths of the three $^{12}CO_2$ peaks across the observed hemisphere of Europa (Fig. 2); the $^{13}CO_2$ feature is too weak for mapping. For the mapping process and at each spatial point, we fitted a model of CO_2 crystalline ice model for the 2.7 μm feature, whereas we modeled the 4.25/4.27 μm double-peaked feature as a combination of two components: CO_2 crystalline ice (using the model described above) and a CO_2 excess. The CO_2 excess model was constructed by subtracting the synthetic spectra of the mixture of CO_2, H_2O and organic molecules, from the crystalline CO_2 spectrum (Fig. 1C). All three bands are strongest in the chaos terrain Tara Regio, and the 2.7 and 4.27 μm CO_2 bands have similar distributions (Fig. 2). The 4.25 μm band has a larger dynamic range, with almost no detection in the northern regions, and a lower abundance between Tara Regio and the anti-Jovian regions (Fig. 2D). The most abundant surface CO_2 appears to be in Tara Regio, potentially indicating this geologically distinct region is associated with an endogenous source of CO_2. The distribution of the 4.25 μm CO_2 band is similar to previous observations of irradiated NaCl on Europa (*11*), whereas the 2.7 μm and 4.27 μm are distributed more broadly across Europa's surface. This is consistent with our interpretation (see above) that the 4.25 μm feature is due to CO_2 mixed with salts or produced via irradiation of carbonate salts.

An endogenous source of CO_2

CO_2 has been observed on a wide variety of Solar System objects and can have either native (endogenous) or non-native (exogenous) origins. The localized CO_2 we observe on Europa could be related to a disrupted surface, with a difference in the surface grain sizes affecting the strength of the CO_2 absorption across the surface (*43*). Exogenous explanations for the observed CO_2 on Europa are possible, but an exogenous source would likely produce a more global distribution, not the observed local concentration that is associated with salts (which are presumably endogenous). CO_2 ice is also localized on Enceladus, where it is known to be endogenous (*44*). Exogenous interplanetary dust grains might deliver carbonaceous material to Europa's icy surface, which could then yield CO_2 through radiolysis (*42*), but no silicate features indicative of such exogenous material have been reported for Europa (*25*). Given the CO_2 association with NaCl, and our laboratory results (*21*), we conclude that the most likely origin of the observed CO_2 is endogenous, at least within Tara Regio.

We consider several possible endogenous sources of CO_2. One possibility is that aqueous solutions rich in CO_2 are present in the subsurface. Such solutions could be present if a long-lived reservoir, such as Europa's ocean, has a low enough pH (*26*), or if fluids migrating through Europa's ice shell incorporate CO_2 derived from destabilized dry ice or CO_2 clathrate hydrate (*45*). A second potential source of CO_2 could be carbonate-bearing fluids (e.g., $NaHCO_3$ or Na_2CO_3 dissolved in water). Enceladus has a carbonate-rich ocean that degases CO_2 (*46*); some of that degassed CO_2 freezes out on the surface (*47*). An analogous process could occur on Europa. Alternatively, endogenous carbonates could react with acid compounds (e.g., H_2SO_4) at or near the surface to produce CO_2, or extruded brines (if they contain (bi)carbonate salts) could produce CO_2 during radiation processing (*48*). A third possibility is that the carbon in the CO_2 might have been from organic compounds that were originally dissolved or suspended in a subsurface liquid water reservoir, which were later converted to CO_2. CO_2 might be generated by irradiation on the surface, when material sourced from Europa's interior, rich in carbonate salts and/or organics mixed with H_2O, is bombarded by charged particles trapped in Jupiter's magnetosphere (*49*). A similar process has been proposed to form hydrogen peroxide (H_2O_2) from H_2O ice; H_2O_2 has previously been observed to be enriched at low latitudes across Europa's leading and anti-Jovian quadrants, including within the boundaries of Tara Regio (*50*). Because the surface environment of Europa is strongly oxidized, CO_2 would be produced by radiation-driven oxidation of reduced carbon species (organics) on Europa's surface; the lack of detectable CO could be an indication of that process (*49*). Regardless of the specific source species of CO_2, we regard the presence of CO_2 in a region with previous indications of subsurface liquid water as evidence of carbon availability in Europa's interior.

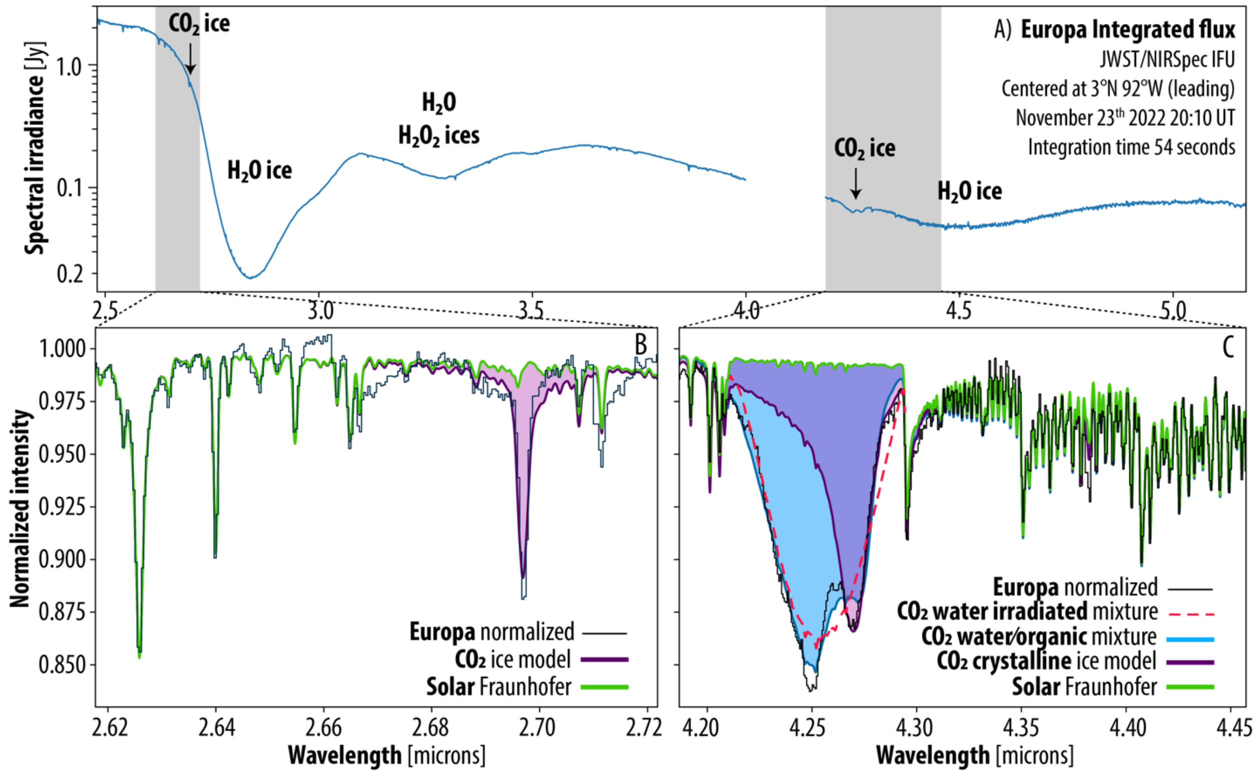

Figure 1: Spectra of Europa's leading hemisphere acquired with JWST. A) Spectrum from 2.5 to 5.2 µm (blue) expressed as spectral irradiance in units of jansky (Jy). Grey shaded regions indicate the ranges plotted in the other panels. Broad features due to H_2O and CO_2 ices are labelled. Narrower features are mostly Fraunhofer lines from sunlight reflected off Europa. B) Zoomed spectrum (black histogram) around the band of crystalline CO_2 ice at 2.7 µm, normalized by the local continuum. The green line shows a solar spectrum, used to identify the Fraunhofer lines. The dark purple line is a model of crystalline CO_2 ice; the light purple shading indicates the integrated band strength used to produce the map in Fig. 2B. C) Same as panel B, but for the double-peaked CO_2 feature at 4.27 µm. The blue line is a model of a CO_2:H_2O:CH_3OH [1:0.8:0.9] mixture at 114 K. The shape of the observed spectrum is fitted with a combination of the blue and purple models. The peak position and width of the feature can alternatively be reproduced by a model (dashed red line) of carbonic acid synthesized in a CO_2:H_2O ice mixture (ratio 5:1) exposed to ionizing radiation.

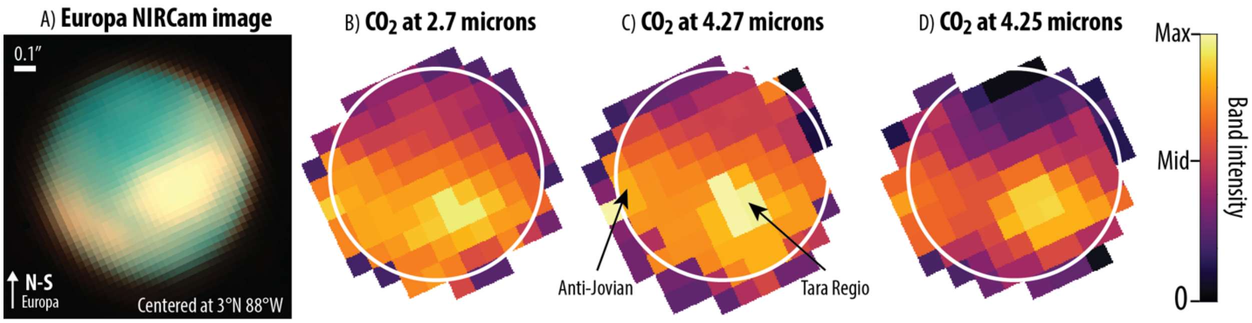

Figure 2: Distribution of CO_2 on Europa. A) A false-color image of Europa as it appeared during the JWST observations (*21*). The image is over-sampled at 0.031″ per pixel; the diffraction-limited resolution is ~0.08″ at these wavelengths. B) Distribution of the band intensity of the CO_2 2.7 µm feature, determined by fitting a model of CO_2 crystalline ice to the spectrum at each location. The white circle indicates the size of Europa in panel A. C-D) The 4.25/4.27 µm double-peaked feature was modeled as a combination of two components: CO_2 crystalline ice (band intensity shown in panel C) and CO_2 non-crystalline ice (band intensity shown panel D). Panels B, C and D share the same color-bar, but with different maximum/middle values of 0.70/0.35, 4.20/2.10 and 7.10/3.55 nm respectively.

References

1. S. M. Howell, The Likely Thickness of Europa's Icy Shell. *Planet. Sci. J.* **2**, 129 (2021).

2. M. G. Kivelson, K. K. Khurana, C. T. Russell, M. Volwerk, R. J. Walker, C. Zimmer, Galileo Magnetometer Measurements: A Stronger Case for a Subsurface Ocean at Europa. *Science*. **289**, 1340–1343 (2000).

3. N. Schilling, F. M. Neubauer, J. Saur, Time-varying interaction of Europa with the jovian magnetosphere: Constraints on the conductivity of Europa's subsurface ocean. *Icarus*. **192**, 41–55 (2007).

4. B. E. Schmidt, D. D. Blankenship, G. W. Patterson, P. M. Schenk, Active formation of 'chaos terrain' over shallow subsurface water on Europa. *Nature*. **479**, 502–505 (2011).

5. P. M. Schenk, C. R. Chapman, K. Zahnle, J. M. Moore, *Ages and interiors: the cratering record of the Galilean satellites.* Jupiter: The planet, satellites and magnetosphere. Edited by Fran Bagenal, Timothy E. Dowling, William B. McKinnon. Cambridge planetary science, Vol. 1, Cambridge, UK: Cambridge University Press, ISBN 0-521-81808-7, p. 427 - 456 (2004).

6. S. A. Fagents, Considerations for effusive cryovolcanism on Europa: The post-Galileo perspective. *Journal of Geophysical Research: Planets*. **108** (2003), doi:10.1029/2003JE002128.

7. R. T. Pappalardo, et al., Geological evidence for solid-state convection in Europa's ice shell. *Nature*. **391**, 365–368 (1998).

8. K. P. Hand, C. F. Chyba, J. C. Priscu, R. W. Carlson, K. H. Nealson, *Astrobiology and the Potential for Life on Europa.* Europa: Edited by Robert T. Pappalardo et al. University of Arizona Press, Tucson. ISBN: 9780816528448 (2009)

9. G. P. Kuiper, Infrared observations of planets and satellites. *The Astronomical Journal*. **62**, 245–245 (1957).

10. M. E. Brown, K. P. Hand, Salts and Radiation Products on the Surface of Europa. *The Astronomical Journal*. **145**, 110 (2013).

11. S. K. Trumbo, M. E. Brown, K. P. Hand, Sodium chloride on the surface of Europa. *Science Advances*. **5**, eaaw7123 (2019).

12. G. B. Hansen, T. B. McCord, Widespread CO2 and other non-ice compounds on the anti-Jovian and trailing sides of Europa from Galileo/NIMS observations. *Geophysical Research Letters*. **35** (2008), doi:10.1029/2007GL031748.

13. N. Ligier, F. Poulet, J. Carter, R. Brunetto, F. Gourgeot, VLT/SINFONI Observations of Europa: New Insights into the Surface Composition. *The Astronomical Journal*. **151**, 163 (2016).

14. T. B. McCord, et al., Non-water-ice constituents in the surface material of the icy Galilean satellites from the Galileo near-infrared mapping spectrometer investigation. *Journal of Geophysical Research: Planets*. **103**, 8603–8626 (1998).

15. L. Roth, J. Saur, K. D. Retherford, D. F. Strobel, P. D. Feldman, M. A. McGrath, F. Nimmo, Transient Water Vapor at Europa's South Pole. *Science*. **343**, 171–174 (2014).

16. X. Jia, M. G. Kivelson, K. K. Khurana, W. S. Kurth, Evidence of a plume on Europa from Galileo magnetic and plasma wave signatures. *Nature Astronomy* **2**, 459–464 (2018).

17. W. B. Sparks, K. P. Hand, M. A. McGrath, E. Bergeron, M. Cracraft, S. E. Deustua, Probing for Evidence of Plumes on Europa with HST/STIS. *Astrophysical Journal*. **829**, 121 (2016).

18. G. Giono, et al. An Analysis of the Statistics and Systematics of Limb Anomaly Detections in HST/STIS Transit Images of Europa. *The Astronomical Journal*. **159**, 155 (2020).

19. L. Paganini, et al., A measurement of water vapour amid a largely quiescent environment on Europa. *Nature Astronomy*. **4**, 266–272 (2020).

20. J. P. Gardner, et al., The James Webb Space Telescope Mission. *Publications of the Astronomical Society of the Pacific*. **135**, 068001 (2023).

21. Materials and Methods are available as supplementary materials.

22. G. L. Villanueva, et al., JWST molecular mapping and characterization of Enceladus' water plume feeding its torus. *Nature Astronomy*. **10** (2023).

23. R. W. Carlson, P. R. Weissman, W. D. Smythe, J. C. Mahoney, The NIMS Science and Engineering Teams, Near-Infrared Mapping Spectrometer experiment on Galileo. *Space Sci Rev*. **60**, 457–502 (1992).

24. R. W. Carlson, et al., Hydrogen Peroxide on the Surface of Europa. *Science*. **283**, 2062–2064 (1999).

25. R. W. Carlson, et al., Europa's Surface Composition. Europa: Edited by Robert T. Pappalardo et al. University of Arizona Press, Tucson. ISBN: 9780816528448 (2009).

26. M. Melwani Daswani, S. D. Vance, M. J. Mayne, C. R. Glein, A Metamorphic Origin for Europa's Ocean. *Geophysical Research Letters*. 48-18, doi:10.1029/2021GL094143 (2021).

27. I. Mishra, et al., A Comprehensive Revisit of Select Galileo/NIMS Observations of Europa. *Planet. Sci. J.* **2**, 183 (2021).

28. R. N. Clark, R. H. Brown, D. P. Cruikshank, G. A. Swayze, Isotopic ratios of Saturn's rings and satellites: Implications for the origin of water and Phoebe. *Icarus*. **321**, 791–802 (2019).

29. T. B. Coplen, et al., Compilation of minimum and maximum isotope ratios of selected elements in naturally occurring terrestrial materials and reagents, *Water-Resources Investigations Report*. U.S. Geological Survey Numbered Series 2001–4222, doi:10.3133/wri014222 (2001).

30. K. A. McCain, et al., Early fluid activity on Ryugu inferred by isotopic analyses of carbonates and magnetite. *Nature Astronomy*. **7**, 309–317 (2023).

31. O. Mousis, J. I. Lunine, A. Aguichine, The Nature and Composition of Jupiter's Building Blocks Derived from the Water Abundance Measurements by the Juno Spacecraft. *Astrophysical Journal Letters*. 918, L23 (2021).

32. C. M. O. Alexander, M. Fogel, H. Yabuta, G. D. Cody, The origin and evolution of chondrites recorded in the elemental and isotopic compositions of their macromolecular organic matter. *Geochimica et Cosmochimica Acta*. **71**, 4380–4403 (2007).

33. J. M. Hayes, K. H. Freeman, B. N. Popp, C. H. Hoham, Compound-specific isotopic analyses: A novel tool for reconstruction of ancient biogeochemical processes. *Organic Geochemistry*. **16**, 1115–1128 (1990).

34. M. van Zuilen, Stable Isotope Ratios as a Biomarker on Mars. *Space Sci Rev*. **135**, 221–232 (2008).

35. G. L. Villanueva, et al., Fundamentals of the Planetary Spectrum Generator: 2022 Edition. ISBN 978-0-578-36143-7 (2022).

36. P. Ehrenfreund, O. Kerkhof, W. A. Schutte, A. C. A. Boogert, P. A. Gerakines, E. Dartois, Laboratory studies of thermally processed H_2O-CH_3OH-CO_2 ice mixtures and their astrophysical implications. *Astron. Astrophys*. 350, 240-253 (1999).

37. J. A. Rathbun, N. J. Rodriguez, J. R. Spencer, Galileo PPR observations of Europa: Hotspot detection limits and surface thermal properties. *Icarus*. **210**, 763–769 (2010).

38. D. P. Cruikshank, et al., Carbon dioxide on the satellites of Saturn: Results from the Cassini VIMS investigation and revisions to the VIMS wavelength scale. *Icarus*. **206**, 561–572 (2010).

39. C. A. Hibbitts, T. B. McCord, G. B. Hansen, Distributions of CO_2 and SO_2 on the surface of Callisto. *Journal of Geophysical Research: Planets*. **105**, 22541–22557 (2000).

40. T. B. McCord, et al., Organics and Other Molecules in the Surfaces of Callisto and Ganymede. *Science*. **278**, 271–275 (1997).

41. B. M. Jones, R. I. Kaiser, G. Strazzulla, Carbonic Acid as a Reserve of Carbon Dioxide on Icy Moons: The Formation of Carbon Dioxide (CO_2) in a Polar Environment. *Astrophysical Journal* **788**, 170 (2014).

42. K. P. Hand, R. W. Carlson, C. F. Chyba, Energy, Chemical Disequilibrium, and Geological Constraints on Europa. *Astrobiology*. **7**, 1006–1022 (2007).

43. R. N. Clark, et al., Compositional mapping of Saturn's satellite Dione with Cassini VIMS and implications of dark material in the Saturn system. *Icarus*. **193**, 372–386 (2008).

44. J.-P. Combe, T. B. McCord, D. L. Matson, T. V. Johnson, A. G. Davies, F. Scipioni, F. Tosi, Nature, distribution and origin of CO_2 on Enceladus. *Icarus*. **317**, 491–508 (2019).

45. N. C. Shibley, G. Laughlin, Do Oceanic Convection and Clathrate Dissociation Drive Europa's Geysers? *Planet. Sci. J.* **2**, 221 (2021).

46. C. R. Glein, J. H. Waite, The Carbonate Geochemistry of Enceladus' Ocean. *Geophysical Research Letters*, 47-3, doi:10.1029/2019GL085885 (2020).

47. R. H. Brown, et al., Composition and Physical Properties of Enceladus' Surface. *Science*. **311**, 1425–1428 (2006).

48. J. F. Cooper, R. E. Johnson, B. H. Mauk, H. B. Garrett, N. Gehrels, Energetic Ion and Electron Irradiation of the Icy Galilean Satellites. *Icarus*. **149**, 133–159 (2001).

49. K. P. Hand, R. W. Carlson, Laboratory spectroscopic analyses of electron irradiated alkanes and alkenes in solar system ices. *Journal of Geophysical Research: Planets*. **117** (2012), doi:10.1029/2011JE003888.

50. S. K. Trumbo, M. E. Brown, K. P. Hand, H_2O_2 within Chaos Terrain on Europa's Leading Hemisphere. *The Astronomical Journal*. **158**, 127 (2019).

51. T. Böker, et al., The Near-Infrared Spectrograph (NIRSpec) on the James Webb Space Telescope - III. Integral-field spectroscopy. *Astronomy & Astrophysics*. **661**, A82 (2022).

52. M. J. Rieke, et al. Performance of NIRCam on JWST in Flight. *Publications of the Astronomical Society of the Pacific*. **135**, 028001 (2023).

53. H. Bushouse, et al., JWST Calibration Pipeline, doi:10.5281/zenodo.7229890 (2022).

54. J. Madden, L. Kaltenegger, A Catalog of Spectra, Albedos, and Colors of Solar System Bodies for Exoplanet Comparison. *Astrobiology*. **18**, 1559–1573 (2018).

55. G. L. Villanueva, M. D. Smith, S. Protopapa, S. Faggi, A. M. Mandell, Planetary Spectrum Generator: An accurate online radiative transfer suite for atmospheres, comets, small bodies

and exoplanets. *Journal of Quantitative Spectroscopy and Radiative Transfer*. **217**, 86–104 (2018).

56. S. Protopapa, et al., Pluto's global surface composition through pixel-by-pixel Hapke modeling of New Horizons Ralph/LEISA data. *Icarus*. **287**, 218–228 (2017).

57. E. Quirico, B. Schmitt, A Spectroscopic Study of CO Diluted in N_2 Ice: Applications for Triton and Pluto. *Icarus*. **128**, 181–188 (1997).

58. G. L. Villanueva, M. J. Mumma, B. P. Bonev, R. E. Novak, R. J. Barber, M. A. Disanti, Water in planetary and cometary atmospheres: H_2O/HDO transmittance and fluorescence models. *Journal of Quantitative Spectroscopy and Radiative Transfer*. **113**, 202–220 (2012).

59. G. L. Villanueva, M. A. Disanti, M. J. Mumma, L.-H. Xu, A Quantum Band Model of the ν_3 Fundamental of Methanol (CH_3OH) and its Application to Fluorescence Spectra of Comets. *The Astrophysical Journal*. **747**, 1–11 (2012).

60. G. L. Villanueva, M. J. Mumma, K. Magee-Sauer, Ethane in planetary and cometary atmospheres: Transmittance and fluorescence models of the ν_7 band at 3.3 μm. *Journal of Geophysical Research*. **116**, 1–23 (2011).

61. C. D. Rodgers, *Inverse Methods for Atmospheric Sounding: Theory and Practice.* World Scientific, ISBN: 978-981-281-371-8 (2000).

62. R. N. Clark, et al., The surface composition of Iapetus: Mapping results from Cassini VIMS. *Icarus*. **218**, 831–860 (2012).

63. W. M. Grundy, L. A. Young, J. R. Spencer, R. E. Johnson, E. F. Young, M. W. Buie, Distributions of H_2O and CO_2 ices on Ariel, Umbriel, Titania, and Oberon from IRTF/SpeX observations. *Icarus*. **184**, 543–555 (2006).

64. R. J. Cartwright, J. P. Emery, A. S. Rivkin, D. E. Trilling, N. Pinilla-Alonso, Distribution of CO_2 ice on the large moons of Uranus and evidence for compositional stratification of their near-surfaces. *Icarus*. **257**, 428–456 (2015).

65. K. P. Hand, R. W. Carlson, Europa's surface color suggests an ocean rich with sodium chloride. *Geophysical Research Letters*. **42**, 3174–3178 (2015).

66. C. J. Bennett, C. Pirim, T. M. Orlando, Space-Weathering of Solar System Bodies: A Laboratory Perspective. *Chem. Rev.* **113**, 9086–9150 (2013).

67. G. Strazzulla, Cosmic ion bombardment of the icy moons of Jupiter. *Nuclear Instruments and Methods in Physics Research Section B: Beam Interactions with Materials and Atoms*. **269**, 842–851 (2011).

68. K. P. Hand, R. W. Carlson, H2O2 production by high-energy electrons on icy satellites as a function of surface temperature and electron flux. *Icarus*. **215**, 226–233 (2011).

69. D. F. Berisford, et al., Erosion of Penitentes Under Experimental Conditions Relevant to Ice-Covered Airless Worlds. *Journal of Geophysical Research: Planets. Vol* 126-10. doi:10.1029/2021JE006955 (2021).

70. M. H. Moore, R. K. Khanna, Infrared and mass spectral studies of proton irradiated H_2O + CO_2 ice: Evidence for carbonic acid. *Spectrochimica Acta Part A: Molecular Spectroscopy*. **47**, 255–262 (1991).

Acknowledgements: This work is based on observations made with the NASA/ESA/CSA James Webb Space Telescope. The data under program ID 1250 were obtained from the Mikulski Archive for Space Telescopes (MAST) at the Space Telescope Science Institute, which is operated by the Association of Universities for Research in Astronomy, Inc., under NASA contract NAS 5-03127 for JWST. We thank Bob Carlson (1941-2022) for assisting in setting the guiding principles of the Europa observational program, and in supporting the experimental framework at JPL that we employed in this work.

Funding: GLV, SF and VK were supported by NASA's Goddard Astrobiology Program, Goddard's Fundamental Laboratory Research (FLaRe), and Sellers Exoplanet Environments Collaboration (SEEC). SNM and HBH acknowledge support from NASA JWST Interdisciplinary Scientist grant 21-SMDSS21-0013. CRG was supported by NASA through Europa Lander funding (award #80NSSC19K0611). KPH acknowledges support from the NASA Astrobiology Program (award #80NSSC19K1427) and the Europa Lander Pre-Project, managed by the Jet Propulsion Laboratory, California Institute of Technology, under a contract with NASA.

Author contributions: GLV, HBH, SNM, KPH, LP, J Stansberry, J Spencer, and GS designed and planned the observations. GLV, SF, VK, RC, J Stansberry, SP and GL analyzed the data, extracted calibrated spectra, produced the maps and performed retrievals. CRG, LR and GCM assisted with discussion and interpretation of the results. All authors contributed to the preparation, writing and editing of the manuscript.

Competing interests: There are no competing interests to declare.

Data and materials availability: The JWST data are available from MAST at https://mast.stsci.edu/ under proposal ID 1250. Our laboratory spectra are provided in Data S1. The data reduction scripts that we developed are available in Data S2.

Supplementary Materials:

Materials and Methods

Figures S1 and S2

Data S1 and S2

References (*50*-*69*)

Supplementary Materials for

Endogenous CO_2 ice on the surface of Europa and no detection of plume activity

G. L. Villanueva, H. B. Hammel, S. N. Milam, S. Faggi, V. Kofman, L. Roth, K. P. Hand, L. Paganini, J. Stansberry, J. Spencer, S. Protopapa, G. Strazzulla, G. Cruz-Mermy, C. R. Glein, R. Cartwright, G. Liuzzi

Corresponding author: geronimo.villanueva@nasa.gov

This PDF file includes:

Materials and Methods
Figs. S1 to S2
Captions for Data S1 to S2

Other supporting files for this paper:

Data S1 (.txt file)
Data S2 (.py file)

Materials and Methods

Data acquisition and analysis

NIRSpec observations were made in integral field unit (IFU) mode (*51*), using three high-resolution gratings (G140H, G235H, G395H) and two detectors per grating (nrs1, nrs2) The resulting data cube has a spatial resolution of 0.1″×0.1″ and a 3″×3″ field of view (FOV). To minimize saturation, we employed the rapid readout and the shortest integration time available for the IFU mode (4×10.74 s), yet most of the G140H/nrs1-nrs2 and G235H/nrs1 exposures were saturated. Fig. 1 shows flux-calibrated spectra for the integrated signal across the Europa disk (~1″ diameter). NIRCam (*52*) observations were made using the sub-array readout (64×72 pixels), with rapid readout and short integration time (50×0.05 s) to minimize saturation.

The data were processed employing the JWST Science Calibration Pipeline (*53*) v1.8.2, and the calibrated frames were analyzed and corrected for dithering and cleaned of bad-pixels using standard data processing methods with scripts available in Data S2. We also validated and benchmarked the flux calibration by comparing to previously reported flux-calibrated low-resolution Europa spectra (*54*). The imaging of Europa was performed by employing two NIRCam filters, F140M [1.331-1.479 µm] and F212N [2.109-2.134 µm]. The two images were combined to compute a false color image of Europa as shown in Fig. 2A, where the green component is F212N, the blue component is 0.7×F140M, and the red component is (F212N - 0.7×F140M)×4.

Spectroscopic interpretation, surface scattering modeling and plume radiative transfer modeling were performed using PSG (*35*, *55*, *56*). Surface reflectances as shown in Fig. 1B-C were modelled using the surface module of PSG that integrates laboratory/model absorbances with optical constants. The reflectance spectrum of crystalline CO_2 as shown in Fig. 1B and Fig. 1C was computed using the optical constants from the SSHADE/GhoSST database (*57*), with the imaginary part of the refractive index includes values derived from a thick crystal at 179 K and from thin films at 28 K. The model of CO_2 water/organic mixture shown Fig. 1C was synthesized using the absorbance laboratory spectrum as reported in (*36*) for a mixture of CO_2, H_2O, and CH_3OH in the ratio 1:0.8:0.9 respectively, measured at a temperature of 114 K. The synthetic reflectance spectrum of irradiated CO_2/water shown in Fig. 1C was computed using the absorbance laboratory spectrum of carbonic acid (H_2CO_3), synthesized in a CO_2:H_2O ice mixture (in the ratio 5:1), then exposed to ionizing radiation in the form of 5 keV electrons (*41*).

These synthetic reflectance spectra were then used to assist with the mapping of the double-peak signal of CO_2 across the moon's surface. Specifically, we defined the CO_2 band in Europa as being composed of two components, a pure crystalline signature (modelled with the SSHADE/GhoSST constants and shown with a 'purple' shading in Fig. 1C) and a residual CO_2 signature, computed as the difference of the CO_2 water/organic model and the pure crystalline model (shown in 'cyan' in Fig. 1C). This is consistent with what is shown in Fig. 1C, in which the 'purple' crystalline signature is largely contained within the CO_2 water/organic signature, with a residual signature shown with a 'cyan' shade. At each spatial location on Europa's surface, we fitted the CO_2 signature as a mixture of these two components and retrieved the band intensity for each component. These integrated band intensities for each component are shown in Fig. 2C-D.

Upper limits on plume or atmospheric molecular species

To search for narrow molecular features, we analyzed the residual spectra over the spectral regions shown in Fig. S1, after subtracting the observed Europa spectra from a continuum model which included solar Fraunhofer lines. The Europa spectral extract was performed over a 1.3” diameter circular aperture over the IFU calibrated frame. The residuals were then compared to synthetic fluorescence emission spectra, by employing a retrieval algorithm. The fluorescence models in PSG account for non-LTE (Local-Thermodynamic-Equilibrium) radiative-transfer effects and incorporate billions of transitions/cascade processes (*58–60*), while the retrieval algorithm in PSG is based on the optimal estimation method (*61*). After each iteration of the retrieval algorithm, a model was constructed, and numerical derivatives were computed for each parameter. This process was repeated until convergence was achieved, and the differences between data and model were minimized. The mean statistical variation of the residual spectra (root-mean-square) was used to quantify the uncertainty (sigma) in the retrieved column densities. As shown in Fig. S1, the residuals are dominated by broad unaccounted features, which probably originate from calibration/instrument issues (e.g., detector readout patterns, fringing) and perhaps weak unidentified ice features.

Laboratory experiments on CO_2 in salt mixtures

Europa’s surface is dominated by water ice (*9*), a complex mixture of other compounds (*14*), including salts (e.g., NaCl, hydrated sulfates) (*10*, *11*), hydrogen peroxide (*24*, *50*) and carbon- (e.g., CO_2) and sulfur-bearing molecular species (*12–14*). Interestingly, CO_2 has been detected beyond Europa on many other Solar System objects, where it has been shown to have both native (endogenous) and non-native (exogenous) origins (*43*, *62–64*). In the case of Europa, the geographic association of irradiated NaCl (*11*, *65*) with the detected CO_2 features as we observe with JWST, could imply an endogenous source from a salty subsurface ocean. The observation of CO_2, but lack of CO, in our JWST spectra could indicate that CO_2 is radiolytically derived from ocean salts or organics, once emplaced on Europa’s irradiated surface. Previous laboratory experiments examined energetic particles irradiating frozen gases. They found that in the presence of water ice, radiolysis produces CO_2 that can be derived from numerous species as a carbon source, ranging from volatile species (e.g. CO and CH_4), to less volatile (e.g. C_6H_6, CH_3OH), to refractory materials, such as asphaltite and amorphous carbon (*66*, *67*).

In order to test the possible state of the observed CO_2 ice, we performed experiments in the Ocean Worlds Lab at JPL (Jet Propulsion Laboratory) (*68*, *69*), with data available in Data S1. Figure S2 shows a comparison between these laboratory experiments and our JWST data. Panels S2A and S2B show the variation of the CO_2 feature as a function of its association with salts, irradiation, and temperature. The salts used were the sea salt mixture ASTM (American Society of Testing and Materials) D 1141-98 Formula a, from Lake Products Company. An ocean mixture was prepared and subjected to a solar irradiance and sublimation stage, which generated a salt evaporite lag that was then directly transferred to the ultra-high vacuum irradiation chamber. The salts were initially irradiated at 10 keV and approximately 30 µA without any CO_2

ice deposited on top and monitored employing an infrared spectrometer. During this time the feature at 4.25 μm emerged, likely from radiolytically processed $NaHCO_3$, which comprised 0.477% by weight of the original salt mixture. We cannot rule out a small contribution from remnant CO_2 contaminant in the vacuum chamber, which was maintained at a pressure of $<10^{-8}$ Torr. After irradiation of the ocean salt evaporite, a CO_2 ice film was vapor deposited on the salt to examine the CO_2 band position.

The feature at 4.25 μm appeared after irradiation of the salts, while the feature at 4.27 μm is from the freshly deposited CO_2. The sample was then irradiated a second time under the same conditions, and the CO_2 features were monitored. The second spectrum (Fig. S2A) shows the resulting modulation of the bands in the 4.25 μm and 4.27 μm regions at 70 K, with the CO_2 ice feature at 4.27 μm appearing stronger. Upon heating to 100 K and 130 K, the spectra show loss of the CO_2 ice but retention of the complexed CO_2 at 4.25 μm, which is likely either adsorbed onto, or captured within, the salts. As the sample temperature increased, the 4.25 μm band strength increased relative to the 4.27 μm band. This higher temperature range is consistent with observations of low latitude daytime temperatures on Europa (*37*) and could be responsible for the structure of the CO_2 absorption feature observed with JWST (Fig. S2C).

Previous experiments showed that CO_2 and water ice mixtures yield a CO_2 band position of 4.269 μm (*70*). In Fig. S2, we observe a slight redward shift of the CO_2 ice feature to 4.277 μm when CO_2 is deposited onto salts and no associated water ice. On Europa, the JWST data at 4.269 μm position could indicate that CO_2 is mixed with water ice.

<u>Isotopic $^{12}C/^{13}C$ ratio of the observed CO_2</u>

After removing the solar features visible in Fig. 1, we obtained the JWST spectrum shown in Fig. S2C. This includes an absorption feature at 4.386 μm due to $^{13}CO_2$ (*70*). The intensity of CO_2 ices features in the 4.2 to 4.4 μm region depends on the host ice matrix and its temperature, however we derive a first approximation of the isotopic ratio from the integrated band intensities. We consider that the model shown in Fig. 1C for crystalline CO_2 is based on optical constants adopting for Earth's isotopic ratio, Vienna Peedee Belemnite [VPDB] with $^{12}C/^{13}C=89.4 \pm 0.2$ (*29*). Using the model spectrum of crystalline CO_2, we derived a band intensity ratio between the $^{12}CO_2$ feature at 4.210 to 4.300 μm and the $^{13}CO_2$ feature at 4.369 to 4.392 μm, measuring a band ratio of 51 ± 10. From the Europa spectrum shown in Fig. S2C, we performed the same integration and obtained a band ratio of 47 ± 9. The $^{13}CO_2$ band is detected at a higher precision on Europa, corresponding to a band ratio of 47 ± 3 when only considering the observational NIRSpec noise of the data. However, the accuracy of this ratio is mostly limited by uncertainties in the baseline definition, and the possible variation of the band ratios for different CO_2 mixtures. By exploring multiple baseline corrections and integration ranges, we estimate that the accuracy of this ratio is ±20% at the 1-sigma level when operating with band integrations. This implies that the $^{12}C/^{13}C$ isotopic ratio of the CO_2 ice on Europa is 83 ± 19, corresponding to a nominal $\delta^{13}C$ ($[^{13}C/^{12}C]_{Europa} / [^{13}C/^{12}C]_{VPDB} - 1$) of +80 ‰.

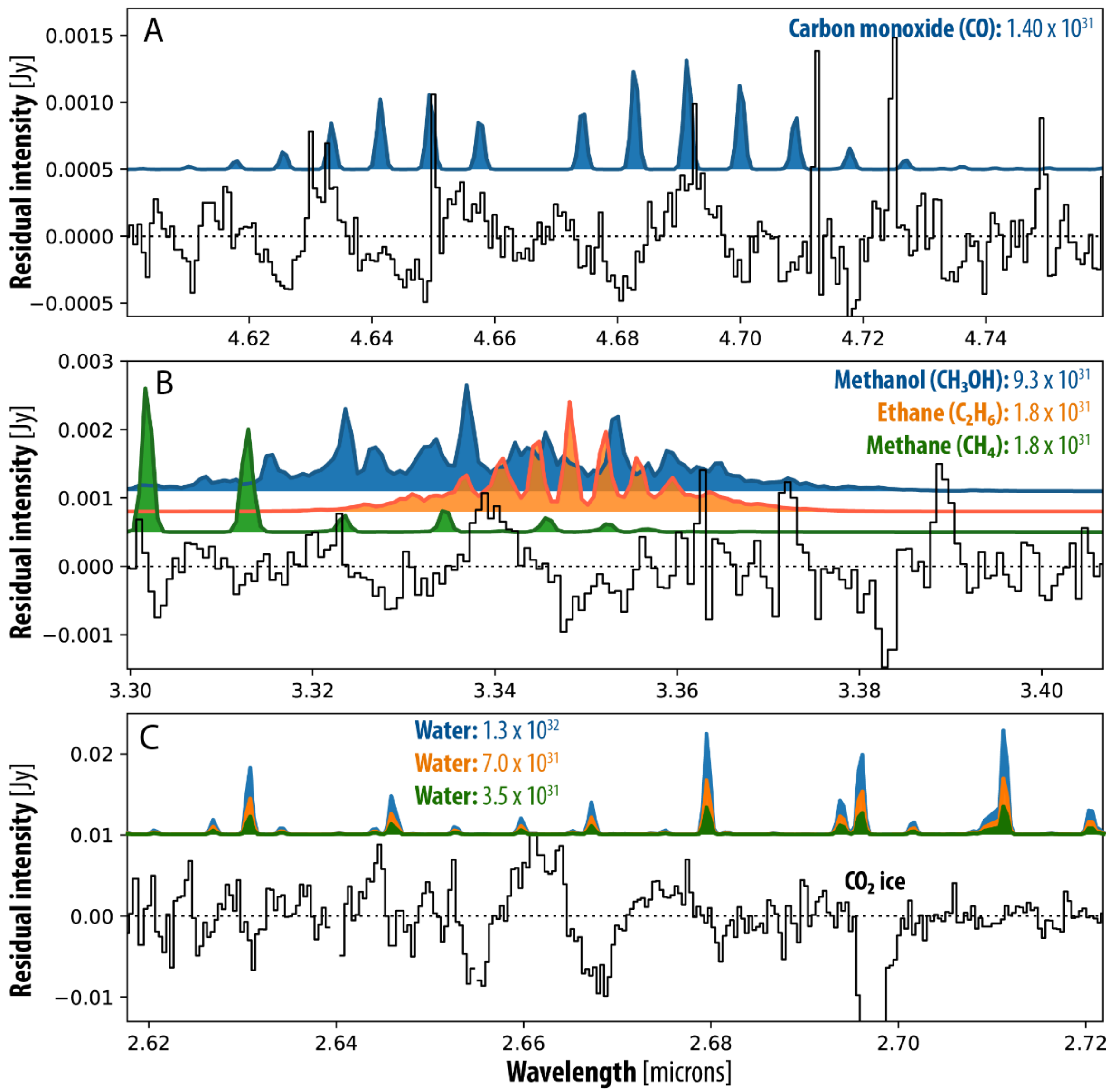

Figure S1: Residual spectra for three spectral regions used to search for CO, CH_3OH, C_2H_6, CH_4 and H_2O molecular emission. In comparison to the observed residual spectra, we show synthetic spectra of molecular fluorescence at different levels of plume abundance. Panel A shows the residuals for CO and the corresponding fluorescence model computed at the determined 3-sigma upper-limit (1.4×10^{31} molecules). This spectral region shows several unaccounted narrow features, not from CO, which are probably related to bad pixels, fringing and/or cosmic-ray hits. Panel B shows the hydrocarbons spectral region, which was used to search for CH_3OH, C_2H_6 and CH_4. The synthetic models were computed considering the corresponding 3-sigma upper-limits number of molecules for each species. Panel C shows the residuals for water, and in green the corresponding model computed at the 3-sigma level (3.5×10^{31} molecules). A model considering the enhanced H_2O levels (7.0×10^{31} molecules) as derived from a previous tentative observation (*19*) is shown in orange, and in blue we show a model considering the activity (1.3×10^{32} molecules) inferred from HST observations (*15*).

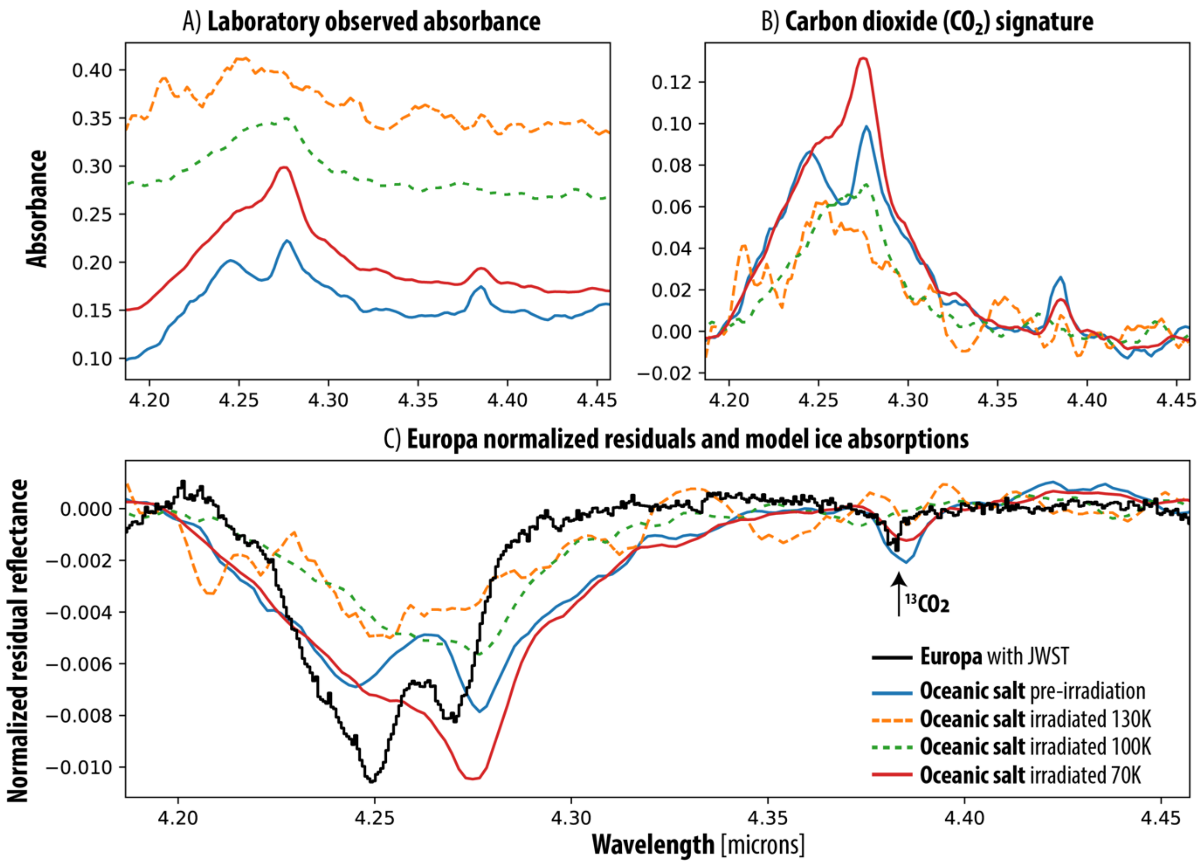

Figure S2: Laboratory spectra of CO_2 oceanic salt complexes and comparison to JWST data. Panel A shows laboratory spectra of oceanic salt evaporite with a CO_2 ice film deposited onto the salts at 10^{-8} Torr and at different temperatures and later being irradiated. For reference, we also show the pre-irradiation sample, which was done with a CO_2 film deposited at 70 K. Panel B shows the CO_2 features as measured from these experiments after subtracting a baseline from the spectra presented in panel A. These absorbance laboratory spectra were used to compute synthetic reflectance spectra with PSG as shown in panel C. Both temperature and irradiation, notably transform the shape of the CO_2 band in the collected laboratory spectra, and in particular the apparent ratio of the 4.25 and 4.27 µm features. Panel C shows these synthetic spectra in comparison to the residual Europa JWST spectrum, derived from Figure 1 after removing and normalizing by a solar continuum model. The double-peak shape of the CO_2 band is observed in both, in the laboratory and in JWST data of Europa, yet the peak at 4.27 µm is shifted relative to the JWST data, which could be related to water ice in the mixture on Europa's surface. A narrow feature observed at 4.386 µm is due to $^{13}CO_2$ ice.